Journal of Inorganic and General Chemistry
ZAAC
Zeitschrift für anorganische und allgemeine Chemie
www.zaac.wiley-vch.de
RESEARCH ARTICLE
Check for updates
DOI: 10.1002/zaac.202200338

Bonding in PdCl(NO) and Related Nitrosylmetal Species of the Enemark–Feltham {MNO}^{10} Type

Daniel Schröder[a] and Peter Klüfers*[a]

Dedicated to Prof. Dr. Wolfgang Beck on the occasion of his 90th birthday.

The crystal-structure analysis of the coordination polymer PdCl(NO) (**1**) by Evers et al. shows a two-dimensional PdCl network of four-coordinate Pd atoms and triply bridging chlorido ligands. The fourth ligand at Pd is a terminally bonded nitrosyl ligand in a bent PdNO function (Pd–N–O = 129°). In terms of the Enemark–Feltham notation, **1** is an {MNO}^{10} compound which leaves a choice regarding the assignment of the ten electrons as d^{10}-Pd^{0}Cl^{-}(NO^{+}), d^{9}-Pd^{I}Cl^{-}(NO) or d^{8}-Pd^{II}Cl^{-}-(NO^{-}) with 0, 1 and 2 electrons allocated at the nitrosyl ligand, respectively. The quantum-chemical treatment by DFT methods and subsequent determination of the oxidation states (OSs) by Salvador's Effective-OS (EOS) method shows highly covalent Pd–NO bonds which narrowly end up on the Pd^{0}Cl^{-}(NO^{+}) side in the course of the OS assignment's heterolytic bond-cleavage procedure. Related halonitrosyls are included to examine the obvious suitability of both linear and bent MNO units as 'ground-state canditates' of {MNO}^{10} systems. Local-mode analysis confirmed the recently formulated weakening of both the metal–nitrosyl and the N–O bond on bending a linear MNO function.

Introduction

A decade ago, Beck et al. published a review devoted to "Nitrosyl Metal Halides and Mass Spectroscopic Support for the Dimeric Structure of $[Ni(NO)I]_2$ and $[Pd(NO)Cl]_2$."[1] With the focus of their work on electron-rich nitrosyl complexes such as the explicitly mentioned compounds in the title, they highlighted a particularly unexplored subset of the halogenido-nitrosyl complexes which is characterised by its specific electron count. In terms of the Enemark–Feltham (EF) notation, both compounds are {MNO}^{10} species. In this notation, the superscript is the number of metal-d-electrons if the NO ligand is taken as NO^{+}.[2] For the example of PdCl(NO), this, for the moment arbitrary, assignment of oxidation states (OSs) results in Pd^{0}Cl^{-}(NO^{+}). For Pd^{0}, the d-electron count is ten, hence the EF-superscript. However, the notation includes alternative distributions for the ten electrons such as Pd^{I}Cl^{-}(NO) or Pd^{II}Cl^{-}(NO^{-}).

Beck's review has remained topical over the last years. To set the scene for this work, we should take a look at Table 2 of the review which compiles the known group-10 nitrosylmetal halogenides.

Reproduction of Table 2 of Ref. [1] "ν(NO) Absorptions/cm^{-1} of nitrosyl nickel and palladium halides (in KBr or Nujol)" (with re-numbered references, re-ordered formulae and comments in footnotes a–e).

NiI(NO)	[3]	1845[a]	PdCl(NO)	[4]	1715,1759[c]
NiBr(NO)	[3]	1872[b]	$[Pd_2Cl_4(NO)_2]^{2-}$	[4b]	1654[d]
$NiCl_2(NO)$	[5]	1835, 1870	$PdCl_2(NO)_2$	[6]	1818, 1833[e]
$NiCl_2(NO)_2$	[7]	1842, 1872			

[a] 1859 cm^{-1} in Ref. [8]; [b] 1870 cm^{-1} in Ref. [8]; [c] IR data from Ref. [4b], 1712 and 1764 cm^{-1} in Ref. [4a]; [d] IR data for the NBu_4 salt in Ref. [4b]; [e] IR values from Ref. [6c] on samples prepared according to Ref. [6a].

A look at the number of the 'Enemark–Feltham electrons' shows that all these species, with the exception of $NiCl_2(NO)$, belong to the 10-electron classes {MNO}^{10} and {M(NO)$_2$}^{10}. (We do not take the {MNO}^{9} outlier $NiCl_2(NO)$ too seriously. It is mentioned as a poorly characterised grey substance in a short notice. Moreover, note the similarity of its IR data with that of $NiCl_2(NO)_2$.) In particular, the mononitrosyls of the {MNO}^{10} class have attracted much interest due to their structural variability. In an attempt to formulate a guideline to {MNO}^{10} structures, Conradie and Ghosh have analysed {NiNO}^{10} as well as related {CuNO}^{10} species.[9] A major focus of their computational analysis is also suited as a common thread for this work. Looking at the compounds of Beck's Table 2, we can expect two bonding modes: linear MNO units with short M–N distances and a relative high energy of the N–O stretch, as well as bent MNO fragments with bond angles of approximately 120° and a markedly red-shifted N–O stretch. In other words, in these electron-rich nitrosyls, both the linear and the bent forms appear as 'ground-state candidates'.

In terms of their frequent occurence, tetrahedral species with linear MNO functions have to be mentioned first (tetrahedral in the broader sense of IUPAC's *T*-4 polyhedral symbol, not only in the strict sense of the cubic *T* groups of group theory). Examples of halogenidonitrosyls include the mononuclear {M(NO)$_3$}^{10} trinitrosyls $[FeBr(NO)_3]$ and $[FeI(NO)_3]$,

[a] D. Schröder, Prof. Dr. P. Klüfers
Department Chemie der Ludwig-Maximilians-Universität
Butenandtstraße 5–13
D-81377 München (Deutschland)
E-mail: kluef@cup.uni-muenchen.de

Supporting information for this article is available on the WWW under https://doi.org/10.1002/zaac.202200338

and the coordination polymer $[\{Co(\mu\text{-}I)(NO)_2\}_{n/n}]$ with infinite Co–I-bonded chains and linear CoNO functions.[10] Related mononuclear mixed carbonyl-nitrosyl species are typical textbook examples such as the triad of *T*-4 species $[Fe(CO)_3(NO)]^-$, $[Fe(CO)_2(NO)_2]$ and $[Fe(CO)(NO)_3]^+$.[11] The dinitrosyl is also part of the tetrad $[Cr(NO)_4]$, $[Mn(CO)(NO)_3]$, $[Fe(CO)_2(NO)_2]$ and $[Co(CO)_3(NO)]$ which collects tetrahedral nitrosyl complexes that are isosteric with the group-10 carbonyl $[Ni(CO)_4]$.[12] Recently, the Krossing group reported another isoelectronic species of the $[Ni(CO)_4]$ parent structure, $[Ni(CO)_3(NO)]^+$.[13] As tetrahedral species, all these compounds comply with a criterion of the Conradie–Ghosh analysis for linear MNO functions: there is no ligand *trans* to the nitrosyl group. However, this criterion is, by no means, commensurate with linear nitrosyl bonding, as is shown by the trigonal-bipyramidal (*TBPY*-5) ion $[Ni(bpy)_2(NO)]^+$ with the nitrosyl ligand in the equatorial plane of the bipyramid. Here, the bent coordination is a result of a delicate balance of orbital interactions, and connects the nickel complex with the isostructural and isoelectronic {CuNO}^{10} dication $[Cu(bpy)_2(NO)]^{2+}$.[9]

Notably, for a trivial reason, none of the species of Beck's 2013 compilation had been considered in Conradie's and Ghosh's 2014 analysis. At that time, none of these compounds, despite, or due to, their simple formulae, had been structurally characterised. Remarkable progress has now been made. In an accompanying publication, Evers et al. report the successful crystallisation and structural analysis of a key compound from this list, PdCl(NO) (**1**).[14] With Evers's work, the remarkably small number of structurally resolved nitrosylpalladium compounds has been enlarged. Restricting ourselves to terminally bonded nitrosyls, we are left, in terms of the CCDC data base, with only four analyses. First, a {PdNO}^{8} species which was claimed by the authors as a $Pd^{IV}(NO^-)$ complex (CCDC code ELALIM).[15] Afterwards, three X-ray investigations (codes EJOREA,[16] XEGMOM,[16b] EJOGEQ[17]) which are devoted to related trinuclear {PdNO}^{10} compounds of the formula $[Pd_3(\eta^2\text{-arene})_2(\mu\text{-}CF_3CO_2)_4(NO)_2]$ were published.

Synthetically, the 10-electron balance of a {PdNO}^{10} species requires a reductant in view of the usual d^8-starting material palladium(II) chloride. Examples include the 1960 method by Smidt and Jira who employed an alkene as an external reductant (inspired by the Wacker process):[4a]

$$PdCl_2 + NO_2^- + RCH{=}CH_2 \rightarrow PdCl(NO) + Cl^- + RCOCH_3$$

The procedure used by Evers et al. was based on a reaction in aqueous solution and uses two electrons of two NO as the reductant:[14]

$$2PdCl_2 + 2NO + H_2O \rightarrow PdCl(NO) + [PdCl_3(NO_2)]^{2-} + 2H^+$$

Remarkably, the latter reaction may be split into a two-step procedure. The first step is the anhydrous reaction of solid $PdCl_2$ and NO gas to another compound tabulated above:[6]

$$PdCl_2 + 2NO \rightarrow PdCl_2(NO)_2$$

The second step is the decomposition of the water-sensitive dinitrosyl under PdCl(NO) precipitation (and decomposition products of the unstable intermediate HNO_2):

$$PdCl_2(NO)_2 + H_2O \rightarrow PdCl(NO) + Cl^- + NO_2^- + 2H^+$$

In this work, the bonding in PdCl(NO) as well as the other entries in Beck's Table 2, above, is analysed by quantum-chemical methods with a focus on oxidation-state and bond-strength considerations. Specifically, we address factors which are responsible for the bend of the PdNO function in mono-, bi- and octanuclear chlorido-terminated cutouts of the PdCl(NO) structure.

Results and Discussion

In **1**, each of the symmetrically equivalent Pd atoms is surrounded by three triply bridging chlorido ligands and a terminal nitrosyl ligand.[14] Figure 1 (left) shows a layer of the two-dimensional PdCl coordination polymer which is wrapped by nitrosyl ligands below and above the layer. We see a pattern of linked binuclear $Pd_2Cl_2(NO)_2$ rhombs as a prominent building block.

Pd–NO bonding in **1** may be analysed by looking at cutouts of the crystal structure of various sizes. The smallest sensible snippet is a mononuclear $[PdCl_3(NO)]^{2-}$ entity with the μ-chlorido ligands of **1** replaced by terminal chlorides. The $[PdCl_3(NO)]^{2-}$ species as well as the related binuclear anion $[Pd_2Cl_2(\mu\text{-}Cl)_2(NO)_2]^{2-}$ are not merely hypothetical species but were mentioned in a work by the Trogler group as entities of Pd/Cl/NO solutions in hydrochloric acid. The authors reported on the low stability of these species which prevented their crystallisation.[4b] Notably, also the binuclear species is a cutout of the crystal structure of **1**. However, both species are only rough approximates of the bonding situation of **1** where no terminal chlorido ligands are present at all. Hence, the bonding analysis was extended to a cutout of four $Pd_2Cl_2(NO)_2$ rhombs which maintained their connection in the crystal structure. In terms of Figure 1 (left), the four centrosymmetric rhombs about $^1/_2$, *y*, *z* with *y*, *z* = $^1/_2$, 0; $^1/_2$, 1; 0, $^1/_2$ and 1, $^1/_2$ were excised and terminated by four chlorido ligands. This octanuclear cutout of the formula $[Pd_8Cl_4(\mu\text{-}Cl_8)(NO)_8]^{4-}$ contains four Pd atoms that bear terminal chlorido ligands but also four Pd atoms that are bonded to bridging chlorides only. Figure 1 (right) shows the octanuclear tetraanion after structural relaxation on the BP86/def2-TZVP + D3 + CPCM(∞) level of theory. The former inversion centres of the rhombs are lost, but the inversion centre of the entire assembly at $^1/_2$,$^1/_2$,$^1/_2$ is preserved and results in the overall C_i symmetry of the tetraanion. Tables 1 and 2 collect significant parameters for the mono-, the bi- and the octanuclear complexes for the chosen theoretical level.

As a convenient reference point of the subsequent discussion on bonding, the tentative low-spin, square-planar {PdNO}^{8} nitrosyl complex $[PdCl_3(NO)]$ was included in Table 1. The d-electron distribution of this [Kr]4d^8 *SP*-4 species is the usual one of a low-spin-d^8 complex, namely $(xy)^2(xz)^2(yz)^2(z^2)^2(x^2-$

Journal of Inorganic and General Chemistry
ZAAC
Zeitschrift für anorganische und allgemeine Chemie

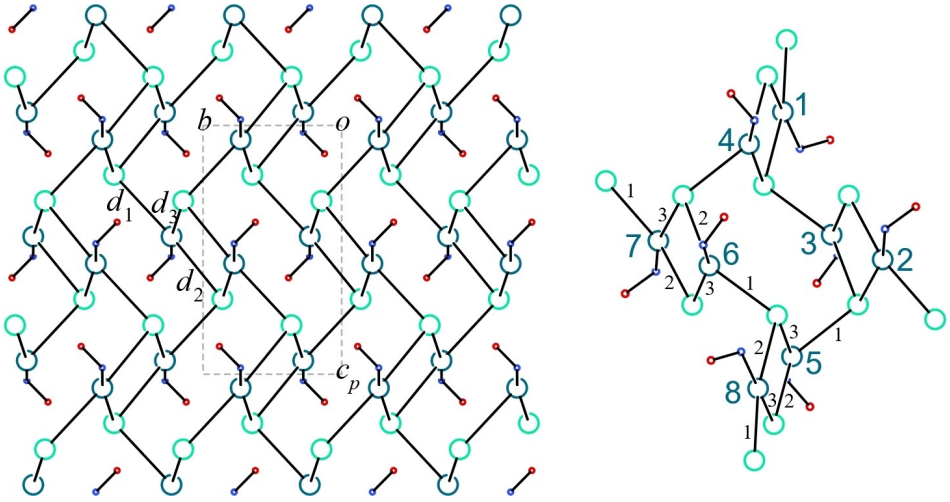

Figure 1. Left: Projection of the major disorder form in the monoclinic structure of **1** ($P2_1/c$) along [100]. The projection of the unit-cell edges with the lengths b and $c_p = c \cdot \sin\beta$ is drawn with dashed lines. Pd–Cl distances d/Å: d_1 2.531, d_2 2.545, d_3 2.596; Pd–N–O: 129°. **Right**: the chlorido-terminated, C_i-symmetric cutout $[Pd_8Cl_4(\mu\text{-}Cl_8)(NO)_8]^{4-}$ after structural relaxation on the BP86/def2-TZVP + D3 + CPCM(∞) level of theory. Pd-numbering 1–8 refers to Table 2, the small numbers are indices n of the d_n distances of Table 2. Colours follow Jmol usage: Pd bluish, Cl green, N blue, O red.

Table 1. BP86/def2-TZVP + D3 + CPCM(∞)-computed values. Charge labels: QTAIM: quantum theory of atoms in molecules; ADCH: atomic dipole-corrected Hirshfeld charge. Local-mode force constants k^a are supplemented by the equivalent local stretch $\tilde{\nu}^a$ for NO. The d_n labels refer to Figure 1. EOS values denote effective oxidation states from the Salvador approach using TFVC-partitioning (see the Experimental Section).

	$[PdCl_3(NO)]$	$[PdCl_3(NO)]^{2-}$	$[Pd_2Cl_4(NO)_2]^{2-}$
$\{MNO\}^n$	$\{PdNO\}^8$	$\{PdNO\}^{10}$	$\{PdNO\}^{10}$
d_{Pd-N}/Å	1.819	1.859	1.870
d_{N-O}/Å	1.117	1.187	1.184
∡ Pd–N–O/°	176.1	124.8	122.5
d_{Pd-Cl}(*trans*)/Å	2.225	2.555	2.579 (d_3)
d_{Pd-Cl}(term-*cis*)/Å	2.346	2.473	2.394 (d_1)
d_{Pd-Cl}(μ-*cis*)/Å			2.490 (d_2)
$\tilde{\nu}_{NO}$/cm^{-1}	2014	1591	1594, 1612
Q_{QTAIM}(Pd)/*e*	0.94	0.56	0.56
Q_{QTAIM}(NO)/*e*	0.31	−0.27	−0.23
Q_{ADCH}(Pd)/*e*	0.46	0.36	0.36
Q_{ADCH}(NO)/*e*	0.46	−0.24	−0.20
k^a_{Pd-N}/N cm^{-1}	2.98	2.26	2.05
k^a_{N-O}/N cm^{-1} ($\tilde{\nu}^a$/cm^{-1})	17.21 (1978)	10.84 (1569)	10.95 (1578)
EOS_{Pd}, EOS_{NO} (R)	+2, +1 (66.0)	0, +1 (62.4)	0, +1 (63.5)

$y^2)^0$. In agreement with the empty d(x^2–y^2) orbital, the Pd–Cl distances are markedly shorter in the $[PdCl_3(NO)]$ species compared with the $[PdCl_3(NO)]^{2-}$ ion. Moreover, the reasons for the linear bonding of the nitrosyl ligand are a key to understanding the bend of the PdNO moiety in the $\{PdNO\}^{10}$ species. Thus, a prerequisite for a linear MNO unit is an empty (or strongly polarised) and accessible metal orbital of the d(x^2–y^2) or d(z^2) type to avoid Pauli repulsion with the lone pair at N (roughly the mixture of NO's 2σ and 3σ MOs) of a formal NO^+ ligand. In the tentative $[PdCl_3(NO)]$, 4d(x^2–y^2) is empty and is thus a suitable acceptor orbital for the nitrosyl lone pair. Next, there should be occupied metal orbitals that act as donor orbitals for the empty N–O(π*) MOs. In $[PdCl_3(NO)]$, this role is taken by the 4d(xz)^2 and the 4d(yz)^2 pairs. Since, on OS determination (see below), these Pd→NO π-bonds are assigned to the metal, these interactions are 'backbonds'.

The contribution of these three interactions to the overall Pd–NO bonding is markedly different. Due to the weak donor character of NO^+, this donor pair is of much less significance for the metal-ligand bond than the same pair of the isoelectronic ligands CO and, in particular, CN^-. The reverse applies to the two empty π* antibonds of these ligands which accept backbonds from the metal. These two backbonds are decisive for a nitrosyl complex. In terms of electron-density shifts on bonding, the backbonds deserve a close look at the electron density distribution along the bonds. Since NO^+ is a distinctly strong

Table 2. BP86/def2-TZVP + D3 + CPCM(∞)-computed values for the C_i-symmetric, {PdNO}^{10}-type $[Pd_8Cl_{12}(NO)_8]^{4-}$ anion and the PdCl(NO) solid. For the various symbols see Table 1. EOS values: 0 for all Pd atoms, +1 for all nitrosyl ligands, R = 66.4 %. Pd numbering refers to Figure 1. The $\mathbf{1}_{calc}$ column lists computed values of the solid **1** taken from Ref. [14].

	terminal Cl Pd2, Pd7	Pd1, Pd8	μ-Cl only Pd3, Pd6	Pd4, Pd5	$\mathbf{1}_{calc}$
d_{Pd-N}/Å	1.855	1.866	1.837	1.839	1.891
d_{N-O}/Å	1.177	1.179	1.172	1.173	1.173
∢ Pd–N–O/°	124.2	123.8	129.3	127.8	123.6
d_1/Å	2.405	2.390	2.505	2.513	2.527
d_2/Å	2.488	2.606	2.517	2.481	2.690
d_3/Å	2.750	2.566	2.569	2.644	2.630
$\tilde{\nu}_{NO}$/cm^{-1}	1635[a]	1626[a]	1654–1676		1688–1765
Q_{QTAIM}(Pd)/e	0.57	0.58	0.61	0.61	0.59
Q_{QTAIM}(NO)/e	−0.18	−0.20	−0.16	−0.17	−0.09
Q_{ADCH}(Pd)/e	0.47	0.37	0.40	0.44	0.34
Q_{ADCH}(NO)/e	−0.16	−0.15	−0.12	−0.12	−0.05
k^a_{Pd-N}/N cm^{-1}	2.08	2.24	1.90	2.47	2.06
k^a_{N-O}/N cm^{-1}	11.45	11.33	11.30	11.73	12.89

[a] Both sym. and asym.

acceptor, it may attract backbonds to such an extent that the electron pairs may become ligand pairs (NO^- or NO^{3-}). This ambiguity will be resolved in the course of the EOS procedure below.

As a first member of the {PdNO}^{10} class, we consider the mononuclear $[PdCl_3(NO)]^{2-}$ species. Here, the standard case of the square-planar low-spin d^8-species $[PdCl_3(NO)]$ is perturbed by two additional electrons which occupy the hitherto empty 4d(x^2–y^2) orbital. Accordingly, the σ-donor pairs of the four ligands of the *xy* plane experience Pauli repulsion. In the case of the chlorido ligands, the Pd–Cl distance increases. For the negligible donor ligand NO^+, however, a mere increase of the Pd–N distance is not a feasable way out since the lengthening of a more or less unimportant σ-bond would destroy the significant π-backbonds. $[PdCl_3(NO)]^{2-}$ chooses a frequent way out. Largely retaining the square-planar coordination, the now occupied 4d(x^2–y^2) pair changes its role from an acceptor to a donor orbital and establishes a σ-(back)bond to one lobe of one of the empty π* acceptor NO–MOs. The second Pd→NO π-backbond is largely unaffected by the bend. A Pd–N–O bond angle of roughly 120° results and, relieving Pauli repulsion, makes the N-based lone pair pass the occupied metal orbitals. (Figure 2 shows the two bonds in a decomposed representation which will be introduced below.)

After having clarified the origin of the bent bonding of the nitrosyl ligand qualitatively, a look at various bond-related measures is appropriate in order to quantify the bonding description. Table 1 shows relevant parameters. Thus, the transition from a linear to a bent PdNO moiety on filling the 4d(x^2–y^2) orbital in the course of the {PdNO}^{8}-to-{PdNO}^{10} two-electron reduction increases the Pd–NO, the N–O and the Pd–Cl distances. The N–O stretch experiences a ca. 400 cm^{-1} redshift. Moreover, weakening of the Pd–NO and the N–O bonds as indicated by the atomic distances is confirmed by the local force constants k^a as a direct measure of bond strength.[18] In terms of charges, one of the two electrons ends up in the

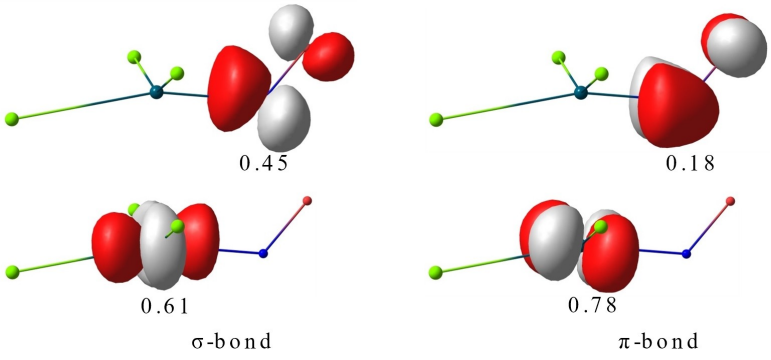

Figure 2. The two decisive Pd–NO bonds in $[PdCl_3(NO)]^{2-}$ (BP86/def2-TZVP). **Left**: the σ-bond in its partitioning into two EFOs, the Pd part with 0.61 electron-pair occupation and the NO contribution with a lower share of 0.45 (note that occupation numbers do not add up precisely to 1.00 due to minor chlorine contributions). **Right**: the π-bond with the respective occupation numbers. CASSCF(4,4) and CASSCF(10,7) approaches shows a more borderline occupation of the σ-bond: Pd 0.52, NO 0.50; π-bond: Pd 0.78, NO 0.19.

PdNO group: in equal parts in terms of QTAIM charges, and in a higher share for NO in terms of Hirshfeld charges. Finally, both charge schemes result in the −0.2 to −0.3 range for the nitrosyl ligand of the mononuclear {PdNO}^{10} species. On proceeding from the mononuclear $[PdCl_3(NO)]^{2-}$ to the dinuclear $[Pd_2Cl_4(NO)]^{2-}$ species, all the values show only slight changes (Table 1).

A closer approach to **1** is achieved with the more extended $[Pd_8Cl_4(\mu\text{-}Cl_8)(NO)_8]^{4-}$ fragment of the crystal structure. Since the symmetry of this octanuclear complex is C_i, there are four independent Pd atoms. Two of them bind a terminal chlorido ligand ('terminal Cl' columns in Table 2), two of them share with the solid **1** exclusive bonding to bridging chlorido ligands ('μ-Cl only' columns).

The various quantitative measures extrapolate the respective small-model values of Table 1. Of special interest are the 'μ-Cl only' entries. The metrical parameters largely resemble those of the solid. Due to the higher charge of the Pd atoms in a bridging-only environment, we find the nitrosyl ligand's charge as the least negative value among the {PdNO}^{10} species. However, the spread is small within the nitrosyl charges of the octanuclear complex. With a mean value of −0.18 *e* and a mean Pd charge of 0.59 *e* (QTAIM values) the question arises of how to assign meaningful oxidation states (OSs).

A rationale for the determination of OSs is presented by a IUPAC recommendation (including two accompanying articles).[19] Here, the electron pair of a bond A–B goes to the atom whose atomic orbital has the higher share in the molecular orbital (MO) which represents the bond. If we asume that the A–B bond is a normal, not coordinative, bond in Haaland's sense, the more electronegative atom will get the bonding pair.[20] The latter statement already dives into the body of practical rules for assigning OSs. If we just look at the wave function, the overall rule is applicable. This approach is used by some recently published algorithms.[21] In this work, we apply Salvador's EOS ('Effective OS') method which is based on a real-space partitioning of the MOs that describe a bond. The principle is demonstrated for the two decisive Pd–NO bonds in the mononuclear model system $[PdCl_3(NO)]^{2-}$. Figure 2 shows these two bonds after the application of the EOS procedure which cuts them to the so-called EFOs (Effective Fragment Orbitals).[22] In the figure, each bond is fragmented into the contribution of the central metal and that of the nitrosyl ligand. The respective weights are given in terms of the fragments' occupation. This occupation number decides the electron pair's assignment in the course of the OS determination. In line with the basic IUPAC concept, the electron pair in question goes to the bonding partner with the higher EFO occupation.

A clear assignment is seen for the π-bond (Figure 2, right). We see a typical backbond as a coordinative bond from a donor orbital of the metal to the acceptor orbital of a π-acidic ligand. Though some electron density is transferred through the backbond (−0.18 *e*×2), the electron pair remains concentrated at the metal and, thus, is counted in favour of the metal on OS assignment. (This is what the term 'backbond' suggests.)

Occupation numbers closer to equality indicate covalency of the A–B bond. As is typical for M–NO σ-bonds, Figure 2 (left) shows a more covalent interaction with an approximately 3:2 share in favour of the metal in the DFT approach, and almost perfect covalence in CASSCF calculations. Hence, though the bond is largely covalent, the electron pair goes to the metal on OS assignment. To sum up, since both Pd–NO bonding pairs go to the metal, the nitrosyl ligand's OS is +1. This statement does not contradict the result of a negative 'real' charge in the −0.1 to −0.3 *e* range. Due to the two-bond scenario, the NO's OS is not simply the nearest integer of its charge. To check this point, we may summarize the occupation numbers of the NO EFOs. With the numbers of Figure 2, the result is 0.45 + 0.18 = 0.63 electron pairs which resembles a charge of 2×(−0.63) *e* = −1.26 *e*. Loading an NO^+ group with −1.26 *e* charges it to −0.26 *e* (confer the QTAIM charge of −0.27 *e* in Table 1). Thus, the nitrosyl ligand is slightly negatively charged but its OS is +1 due to the definition of an OS as a winner-take-all principle per bond in the framework of a two-bond scenario. As a result, all the molecular entities investigated in this part are Pd^0/NO^+ species. Notably, all the species of this work confirm recent results showing that there is no justification to consider a bent-bonded nitrosyl to be a singlet NO^- ligand with the only argument that the MNO link is bent.[23]

Table 2 of Beck's compilation, we reproduced above, contains two more palladium species, both closely related to **1**. The first has already been considered, the chlorido-terminated binuclear anion $[Pd_2Cl_4(NO)_2]^{2-}$. The N–O stretch of this species has been reported by Trogler as 1654 cm^{-1} for the tetrabutylammonium salt, compare 1597 and 1614 cm^{-1} in Table 1. The second Pd species is the reactive dinitrosyl $[PdCl_2(NO)_2]$ which decomposes in water under formation of **1** (see the Introduction). The left column of the compilation shows nickel compounds which are well-suited to compare the various binding modes of a nitrosyl. Specifically, we see the compounds NiI(NO) and NiBr(NO). We skip the $NiCl_2(NO)$ entry for reasons explained in the Introduction. Finally, there is a dinitrosyl, $NiCl_2(NO)_2$.

For the dinitrosyl couple, $[NiCl_2(NO)_2]$ and $[PdCl_2(NO)_2]$, the literature provides us with two values for the N–O stretches each, an asymmetrically and a symmetrically coupled valence vibration. Attempts to model these tentatively mononuclear dinitrosyls give a first insight but leave questions open for future experimental clarification. On appraising the limited experimental data, a computational survey should restrict itself to simply clarifying the nitrosyls' bonding mode—linear or bent? For both central metals the matter is quite clear: when linear bonding is enforced via angle constraints, unstable species with negative frequencies of bending vibrations result. On unconstrained relaxation, species of the bent class are then obtained. Local minima are found for all the possible combinations *anti*/*anti*, *anti*/*syn*, *syn*/*syn* with *anti* and *syn* referring to the respective tilt of a nitrosyl away or towards the bisector of the N–M–N angle. For both the BP86 and the TPSS functional (+def2-TZVP + D3), the *anti*/*anti* isomer is both the most stable one and shows the best match between experimental and calculated N–O stretches. Table 3 shows these values with the better match for the palladium compound. The limited

Table 3. Experimental and computed values for the N–O stretches of the *anti*/*anti* isomers of $[MCl_2(NO)_2]$ (M = Ni, Pd) dinitrosyls on the BP86/def2-TZVP + D3 level of theory. Angles are tabulated which show the extent of the MNO bend as well as the deviation of these C_{2v}-symmetric *T*-4 structures from the tetrahedral angle.

	$[NiCl_2(NO)_2]$	$[PdCl_2(NO)_2]$
exp.:		
$\tilde{\nu}_{asym}/cm^{-1}$	1842	1818
$\tilde{\nu}_{sym}/cm^{-1}$	1872	1833
calc.:		
$\tilde{\nu}_{asym}/cm^{-1}$	1780	1775
$\tilde{\nu}_{sym}/cm^{-1}$	1835	1819
∡ M–N–O/°	125.1	120.5
∡ N–M–N/°	97.2	90.2
∡ Cl–M–Cl/°	127.1	137.1

reliability of the sparsely reported data for the nickel compound should be considered as well.

Compared with the uncertainty of the dinitrosyl treatment, nickel analogues with **1** provide more consistent data. Both NiBr(NO) and NiI(NO) have been tentatively seen either as tetrameric species with an Ni_4X_4 heterocubane core or as dimers with an Ni_2X_2 core (of unspecified structure) and terminal nitrosyl ligands in all cases.[1,3] In fact, computation is in line with these assumptions but cannot decide between the cases. Table 4 shows the matching experimental and computed N–O stretches of both compounds and includes the values of the tentative chlorido homologue.

The minimum structures of the dimer computations show butterfly-shaped $Ni_2(\mu\text{–}X)_2$ cores instead of plane M_2X_2 rhombs as found in **1** and the cut-outs thereof. The three heterocubane species exhibit T_d symmetry. The relaxed T_d structures do not show negative frequencies; moreover, we arrive at them starting from initially bent structures. T_d symmetry implies strictly linear M–N–O linkages. The symmetry species for the IR-allowed asymmetric stretch is T_1 (the computed totally symmetric, IR-forbidden A_1 vibration is tabulated as well).

Notably, the formulation as a heterocubane-type tetramer is not decisive for the MNO linearity. On additionally refining a tentative $[\{PdCl(NO)\}_4]$ homologue, the T_d form is no longer the ground state but a transition state, 43.1 kJ mol^{-1} above the GS. The GS is made up of bent-bonded PdNO functions that complete a Pd_4Cl_4 heterocubane core. However, though bent, it should be noted that the Pd–N–O angle is enlarged compared to others of this work. Table 5 collects significant bonding parameters which allow a look at the typical characteristics of linear and bent bonding in an isomeric couple. First, the charge of the nitrosyl ligands is almost the same for both forms. Second, the local force constants k^a indicate a bond weakening of both the Pd–N and the N–O bond in the bent form as is known from {CoNO}[8] and {RuNO}[6] species.[23d]

Though all the species of Table 4 are either tentative or waiting for experimental verification, the computations nicely show the structural variability of {MNO}[10] coordination entities. There are two choices which are represented by $[\{NiCl(NO)\}_4]$ and its heavier homologue $[\{PdCl(NO)\}_4]$. As a 3d central metal, nickel has rather contracted d-orbitals. As a result, a short Ni–NO distance is essential to create enough overlap in the decisive Ni→NO backbonds. The interfering Pauli repulsion between the NO lone pair and occupied Ni AOs is lifted in the acentric structure by admixture of an empty Ni($4p_z$) orbital to 3d(z^2) (assuming the Ni–N–O axis as *z*) which polarises the Ni pair to the opposite side of the metal core. It has been highlighted in the Introduction that all the mixed carbonyl-nitrosyl complexes with a ten-electron balance belong to this linear subtype.

The other choice is made by Pd where higher stability of the PdNO moiety is gained by using 4d(z^2) to establish a σ-backbond as described above. The delicacy of the balance between the two bonding modes is nicely demonstrated by recently published halonitrosyls of the {MNO}[10] type with copper as the central atom. Both $[CuCl_3(NO)]^-$ and $[CuBr_3(NO)]^-$ were found to be isostructural with the bent-type $[PdCl_3(NO)]^{2-}$ species of this work.[24]

Table 4. The T_d-symmetric heterocubane-type $[\{Ni(\mu_3\text{-}X)(NO)\}_4]$ tetramers and the C_{2v}-symmetric, butterfly-shaped $[\{Ni(\mu\text{-}X)(NO)\}_2]$ dimers of Ni(NO)X (X = Cl, Br, I); all calculations on the BP86/def2-TZVP + D3 level of theory. For $n = 2$, δ is the dihedral angle between the two $Ni(\mu\text{-}X)_2$ triangles of the butterfly-shaped $Ni_2(\mu\text{-}X)_2$ cores.

	$[\{NiCl(NO)\}_n]$	$[\{NiBr(NO)\}_n]$	$[\{NiI(NO)\}_n]$
$\tilde{\nu}_{asym}/cm^{-1}$ (exp)	–	1872	1845
calc. for $n = 2$:			
$\tilde{\nu}_{asym}/cm^{-1}$	1874	1867	1850
$\tilde{\nu}_{sym}/cm^{-1}$	1900	1892	1876
∡ M–N–O/°	176.5	175.2	169.5
δ/°	132.3	126.7	112.1
calc. for $n = 4$:			
$\tilde{\nu}(T_1)/cm^{-1}$	1875	1868	1853
$\tilde{\nu}(A_1)/cm^{-1}$	1897	1889	1872
∡ M–N–O/°	180.0	180.0	180.0

Table 5. The tentative heterocubane-type tetramer of PdCl(NO); all calculations on the BP86/def2-TZVP + D3 level of theory. The $[\{PdCl(NO)\}_4]$ column refers to the bent-type ground state, the $[\{PdCl(NO)\}_4]^{TS}$ column to the linear-type, T_d-symmetric, transition state.

	$[\{PdCl(NO)\}_4]$	$[\{PdCl(NO)\}_4]^{TS}$
$\tilde{\nu}_{asym}/cm^{-1}$ (calc)	1786	1853
$\tilde{\nu}_{sym}/cm^{-1}$ (calc)	1809	1878
∡ Pd–N–O/°	141.7	180.0
d_{Pd-N}/Å	1.794	1.782
d_{N-O}/Å	1.162	1.156
$Q_{QTAIM}(NO)/e$	−0.132	−0.145
k^a(N–O)/N cm^{-1}	13.52	14.21
k^a(Pd–N)/N cm^{-1}	3.73	4.12

Conclusion

In conclusion, we confirmed that the coordination polymer PdCl(NO) (**1**), more precisely [{Pd(μ_3-Cl)(NO-κ*N*)}$_{n/n}$], along with various chlorido-terminated molecular cut-outs belong to a specific subclass of the electron-rich {PdNO}^{10} compounds which is characterised by markedly bent PdNO moieties (Pd–N–O ≈ 120°). In terms of oxidation states, the ten-electron balance is achieved by the OS distribution Pd^0(NO$^+$). Thus, **1** is another example for a bent-bonded nitrosyl ligand which is not in the ^{1}NO$^-$ state in terms of a wave-function-based method for OS determination.[23] Taking Table 2 of Beck's 2013 compilation of group-10 halonitrosyls, bent MNO units appear to be a standard for {Pd(NO)$_n$}^{10} (n = 1 or 2) species, whereas homologuous nickel compounds tend to linear ground states in {NiNO}^{10} entities.

Experimental Section

Structure optimisations and analytical frequency analyses of all species were performed by ORCA, version 5.0.3,[25] using the Karlsruhe def2 basis sets,[26] their auxiliary basis def2/J,[27] the GGA density functional BP86 (or the meta-GGA functional TPSS),[28] the Becke-Johnson-damped D3 dispersion correction,[29] the implicit solvation model CPCM for charged species,[30] and the integration acceleration method RI.[31] For a check of triplet stability, the hybrid functional TPSSh was used to avoid the known singlet bias of BP86. CPCM(∞) was used for all charged species to simulate the crystal environment.

Local-mode analysis was performed by LModeA 2.0.0 after adaption of the input routine to the format of ORCA 4/5 hessians.[32] QTAIM analyses were performed using MultiWFN 3.8.[33] The converged wave functions of the ORCA calculations were converted via orca_2mkl from the gbw files to MultiWFN-compatible molden files in order to prepare formatted Gaussian-checkpoint files (fchk) files for TFVC-derived EOSs (Topological Fuzzy Voronoi Cells). Then, the fchk file was passed to the APOST-3D 4.0 program,[34] together with an input file which specified the fragmentation, yielding the effective fragment orbital (EFO) occupations and finally the oxidation state of each fragment. The background of EOS-related computations in the field of nitrosyl complexes including the definition of the tabulated values R is given in the Experimental Section of Ref. [23b]. The EOS method itself is introduced and compared with other methods in Refs. [21].

Appendix I

Are the {MNO}^{10} systems of this work adequately described as closed-shell (cs) singlets in view of the small band gap of the PdCl(NO) parent compound? This question arose in the course of the reviewing process. In view of the small band gap of the solid, a referee expected such a small HOMO/LUMO gap in the model compounds, specifically in the octanuclear cutout, so that close-lying excited states, including non-singlets, might mix into the DFT-computed ground state. As a matter of fact, these doubts include the nickel species of this work.

To check these objections, the reviewer suggested that we apply the coupled-cluster-derived T_1 diagnostics to determine the extent of multireference character. Since these aspects depart from the common thread of this work, they have been dealt with in this appendix which is organised as follows:

(1) The HOMO/LUMO gap of the palladium key species of this work was investigated by TDDFT calculations and presented in terms of the computed absorption spectra of the visible region.
(2) The closed-shell singlet wave functions of key species were checked with respect to restricted/unrestricted instabilities. From this point on, the nickel compound [NiCl$_2$(NO)$_2$] was included. To allow for comparison with a well-investigated {MNO}^{10} species, values for the prototypic nitrosylferrate [Fe(CO)$_3$(NO)]$^-$ were included as well, if helpful.[23d,35]
(3) The triplet states of [PdCl$_3$(NO)]$^{2-}$ and [NiCl$_2$(NO)$_2$] were investigated.
(4) The recommended T_1 diagnostics as well as the in our eyes more informative finite-temperature-DFT-derived FOD analysis by Grimme were used as measures of the potential multireference character.
(5) After demonstrating that static correlation within the M(NO) moieties was responsible for the increased MR measures, a CASSCF approach was used to quantify the multireference extent.
(6) Finally, the trace of static correlation in the DFT treatment was addressed.

(1) Excited states of the {PdNO}^{10} species

PdCl(NO) is black. Experimentally as well as computationally the colour goes along with a small band gap of only 0.3 eV of the solid which resembles a wavenumber of about 2400 cm^{-1} in the IR region of the electromagnetic spectrum.[14] On increasing radiation energy, the absorption coefficient remains small in the low-energy region until the onset of more intense absorptions is reached at ca. 1.3 eV. The mono-, di-, and octanuclear cutouts of the PdCl(NO) solid share the 1.3 eV onset but not the low-energy absorption, as shown by the absorption spectra of the model species in a TDDFT approach (Figure 3).

The excitations of the three species share some details: the acceptor MOs of the visible region are exclusively the two (Pd$_1$), four (Pd$_2$), or 16 (Pd$_8$) Pd–NO antibonding MOs with the Pd–NO π-antibond(s) as the energetically lower half, and the Pd–NO σ-antibond(s) as the higher half. For all three species, the HOMO is a Pd–NO σ-bonding MO, the HOMO→LUMO excitation thus shifts an electron from the Pd–NO σ-bond to the Pd–NO π-antibond. For all three species, the next absorption bands stem from Pd–Cl π-antibonds as electron donors to the same acceptors. With the higher share of the NO ligand in the acceptor MOs, all excitations have some metal-to-ligand charge-transfer character. Note that the absorption onset is slightly red-shifted with increasing nuclearity. For the Pd$_8$ species, the HOMO/LUMO transition is computed at 1.28 eV = 10322 cm^{-1} and thus coincides with a marked increase of the absorption in the solid-state spectrum of PdCl(NO).[14] Hence, the small band gap of solid PdCl(NO) should be caused by transitions which we do not see in the low-molecular cutouts.

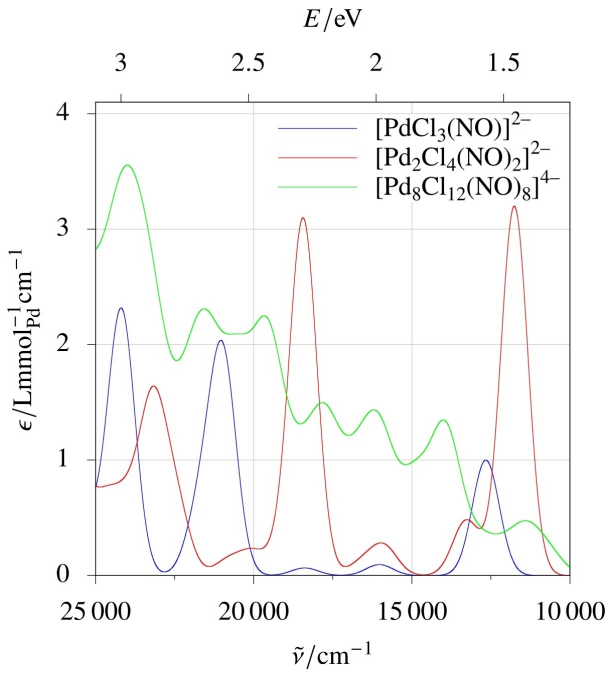

Figure 3. The BP86/def2-TZVP + CPCM-computed, Gauss-broadened vis-NIR spectra of the PdCl(NO) model species.

In fact, the authors of Ref. [14] identify them as excitations within the extended PdCl layers of the solid.

(2) Wave-function stability of mononuclear nitrosyls

The check for wave-function stability as implemented in Orca was performed for the mononuclear nitrosyl palladium species, the nickel dinitrosyl, and, as a reference, the tricarbonylnitrosylferrate(1−) anion.

Table 6 shows the result. For the three investigated functionals, the cs-singlet wave function of the Pd species was stable, whereas even the small HF share of TPSSh resulted in a restricted/unrestricted instability for the nickel dinitrosyl. The reference ferrate species's cs-TPSSh wave function was stable but unstable for the range-separated functional.

For a closed-shell transition-metal compound, the higher stability of an unrestricted wave function requires the check of two issues. First, the existence of low-lying triplets. Thus, in a recent work, values of $\langle S^2 \rangle \neq 0$ have been computed for singlet low-spin states if the corresponding high-spin species were more stable than the singlet.[36] (The range-separated CAM-B3LYP functional was included in Table 6 for comparison with this work.) However, in the case of the $\{M(NO)_n\}^{10}$ species, triplet admixture appears unfavourable in terms of the triplet energies. We will investigate this point in the following section (after the T_1 diagnostics) and proceed here with a second possible reason for an RHF/UHF instability, namely the higher stability of a singlet biradical over the cs-singlet.

We checked this point for the unstable wave function of the cs-TPSSh computation on $[NiCl_2(NO)_2]$ by a broken-symmetry (bs) approach. As expected, a stable bs-solution was obtained, 7.4 kJ mol^{-1} below the cs-singlet (corresponding-orbital overlap for the HOMO and the HOMO−1: 0.84 and 0.88, respectively).

Table 7 shows mostly marginal differences in selected metrical and spectroscopic values. As an exception, the Ni–N distance is markedly elongated in the bs-calculation. Notably, the cs-value resembles the Ni–N distance of the cs-BP86 approach (which passed the wave-function stability test) of 1.814 Å. (In agreement with the stable cs-BP86 singlet wave function, a bs-BP86 treatment falls back to the cs-singlet.) In the CASSCF section below, we will return to this point and explain the nitrosyl-typical too short M–NO distances in cs-DFT calculations as the trace of a Pauli-repulsion-caused weakening of an M–NO bond which manifests itself computationally as static correlation. However, before treating this common characteristic of metal nitrosyls, we have to settle the objection that triplet states may be of significance for the $\{M(NO)_n\}^{10}$ ground-state description.

(3) Triplet states of $[PdCl_3(NO)]^{2-}$ and $[NiCl_2(NO)_2]$

For the moment, both $[PdCl_3(NO)]^{2-}$ and $[NiCl_2(NO)_2]$ are closed-shell $\{M(NO)_n\}^{10}$ species. As such, a metal-centred triplet state requires a 4d-to-5s transition for Pd and a 3d-to-4s transition for the nickel compound. With a nitrosyl complex, energetically lower-lying, charge-transfer-related triplets are expected in view of the TDDFT analysis. Since all the computed excitations of the visible region populate the N–O-π* orbital, the searched-for triplets may be formulated starting from these spin-allowed low-energetic transitions with subsequent intersystem crossing to the triplet. Since the transitions populate the Pd–NO-

Table 6. $\langle S^2 \rangle$ values as a measure of spin contamination of the unrestricted singlet wave function; "–" indicates stability of the cs-singlet. Note the dependence of spin contamination on the functional's HF admixture (% HF: BP86 0, TPSSh 10, CAM-B3LYP 19-65).

	BP86	TPSSh	CAM-B3LYP
$[PdCl_3(NO)]^{2-}$	–	–	–
$[NiCl_2(NO)_2]$	–	0.524	1.297
$[Fe(CO)_3(NO)]^-$	–	–	0.450

Table 7. Parameters of the cs- and the bs-singlet from TPSSh/def2-TZVP + D3 calculations on the most stable isomer of $[NiCl_2(NO)_2]$, the *anti/anti* form with both NOs tilted away from the N–Ni–N bisector. Atomic distances and wavenumbers of the N–O stretch.

	cs-TPSSh	bs-TPSSh
d_{Ni-N}/Å	1.817	1.863
d_{N-O}/Å	1.139	1.140
d_{Ni-Cl}/Å	2.130	2.138
∡ Ni–N–O/°	122.1	122.4
$\tilde{\nu}_{NO,\,asym}$/cm^{-1}	1851	1859
$\tilde{\nu}_{NO,\,sym}$/cm^{-1}	1910	1917

Table 8. $[PdCl_3(NO)]^{2-}$. Atomic distances and wavenumbers of the N–O stretch: BP86/def2-TZVP. Energies: canonical CCSD(T) extrapolated to the basis-set limit via def2-DZVP and def2-TZVP, TPSSh reference wave function; CPCM applied for both methods.

	singlet	triplet
d_{Pd-N}/Å	1.860	1.995
d_{N-O}/Å	1.187	1.221
$\tilde{\nu}_{NO}$/cm^{-1}	1594	1475
$E_{vertical}$/kJ mol^{-1}	0	114.1
$E_{adiabatic}$/kJ mol^{-1}	0	90.3

Table 9. The T_1 diagnostic and N_{FOD} values as indicators of static correlation. T_1 from canonical CCSD(T) and the DLPNO variant; all T_1 values refer to the def2-TZVP basis set. N_{FOD} values from a BHLYP/def2-TZVP computation with an electronic temperature of 15000 K as recommended in Ref. [38]. Note the size inconsistency of N_{FOD}; division by the nuclearity n very roughly yields comparable values.

M_n species	T_1	DPLNO-T_1	N_{FOD}
$[PdCl_3(NO)]^{2-}$	0.0399	0.0280	1.371
$[Pd_2Cl_4(NO)_2]^{2-}$	0.0432	0.0305	2.278
$[Pd_8Cl_{12}(NO)_8]^{4-}$		0.0334	8.317
$[NiCl_2(NO)_2]$	0.0964	0.0556	1.672
$[Fe(CO)_3(NO)]^-$	0.0609	0.0514	1.175

antibonding LUMO and LUMO + 1, they should result in a marked weakening of the Pd–NO bond and a marked overall instability of the triplet. In fact, this expectation is confirmed by computation. Table 8 illustrates these qualitative statements in terms of quantitative measures. For $[PdCl_3(NO)]^{2-}$, a DFT approach shows the lengthening of both the Pd–N and the N–O bond as well as a marked red-shift of the triplet's N–O stretch. The corresponding energies show the triplet instability directly. Table 8 shows both the vertical transition as well as the adiabatic value, the energy difference between the singlet and the structurally relaxed triplet, both from a coupled-cluster analysis on the CCSD(T) level.

Similar values are obtained for $[NiCl_2(NO)_2]$. The vertical and adiabatic transitions need 112.2 kJ mol^{-1} and 84.3 kJ mol^{-1}, respectively, and are thus in the same range as the palladium homologue (the corrected ground state from the stability analysis was used as the reference wave function of the Ni species). Note that the usual difference between a 3d and a 4d central metal must not be expected for those two dinitrosyls since the triplets are not metal-centred. As an overall result of our analysis, we see singlet ground states without considerable triplet admixture due to the marked instability of the latter.

(4) T1 diagnostics and FOD

The recommended T_1 diagnostic as a measure of multireference character (after having excluded triplets: the singlet-biradical character) is reported in Table 9 for the $\{PdNO\}^{10}$ species of this work as well as for the nickel dinitrosyl. In addition, values for the nitrosylferrate $[Fe(CO)_3(NO)]^-$ may help to compare the new species with a well-known nitrosyl. For the evaluation of the result see Ref. [37]. Published limits for significant multireference character depend on the chosen coupled-cluster variant and the reference wave function. To account for these effects, Table 9 lists the T_1 diagnostic for the canonical CCSD(T) approach for the smaller species. Lower values are expected for the DLPNO variant of CCSD(T) which was applied to the large Pd_8 species exclusively.[37a] Instead of the TPSSh reference wave function used for the above-listed energies, a HF reference was used for the T_1 diagnostic. (DFT references which [partly] capture multireference character usually result in markedly lower values; for example 0.0155 for the Pd_1 species with the TPSSh reference, 0.0260 for the nickel dinitrosyl).

Using T_1 as a measure of static correlation leaves us with the open question: at which positions does a species show an increased multireference character? Here, another measure is more expressive than the T_1 diagnostic, namely Grimme's FOD analysis.[38] Alongside with a numerical parameter N_{FOD} (Table 9), ρ_{FOD} surfaces directly show the "hot", the correlated, electrons. Figures 4–7 show such surfaces for the isovalue recommended in Ref. [38] of 0.005 e a_0^{-3}. In addition, the higher value of 0.008 e a_0^{-3} is chosen to show the functional groups most affected by static correlation. It is obvious that it is the MNO function in all cases (note the included FOD-derived frontier-orbital occupations which give a rough 'outlook' at the CASSCF occupations below). Included is the graph for $[Fe(CO)_3(NO)]^-$ to demonstrate that the species of this work show the usual properties of a metal nitrosyl.

With these data, the final steps were done, CASSCF calculations on the mononuclear species.

(5) CASSCF

Using the FOD-intensive MOs for the palladium species, a CASSCF(4,4) approach appears to be the smallest sensible choice for a Pd(NO) function (8,8 for the nickel dinitrosyl). Figure 8 shows the result for the $[PdCl_3(NO)]^{2-}$ species. As usual

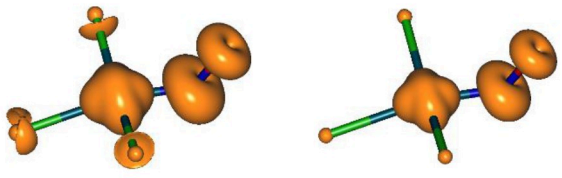

Figure 4. The $\rho_{FOD} = 0.005$ e a_0^{-3} (left) and 0.008 e a_0^{-3} (right) surfaces of $[PdCl_3(NO)]^{2-}$. The Pd–NO σ-bond is most affected by static correlation with bond and antibond occupations of 1.79 and 0.22, respectively.

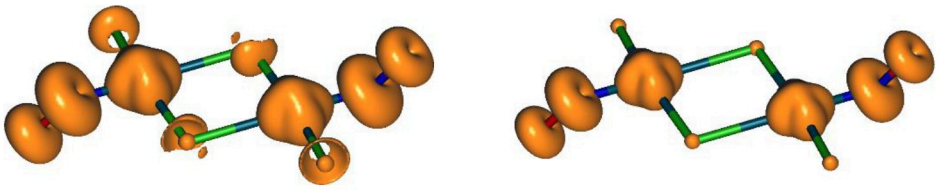

Figure 5. The $\rho_{FOD} = 0.005$ e a_0^{-3} (left) and 0.008 e a_0^{-3} (right) surface of $[Pd_2Cl_4(NO)_2]^{2-}$. Occupations of MOs related to σ-bonds 1.75 and 1.79, to σ-antibonds 0.20 and 0.18.

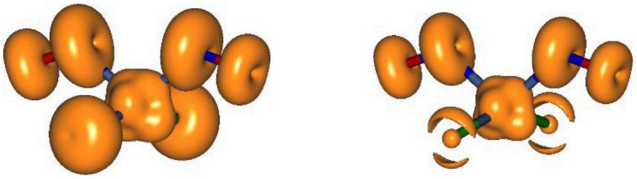

Figure 6. The $\rho_{FOD} = 0.005$ e a_0^{-3} (left) and 0.008 e a_0^{-3} (right) surface of $[NiCl_2(NO)_2]$. Occupations of MOs related to σ-bonds 1.70, to σ-antibonds 0.26.

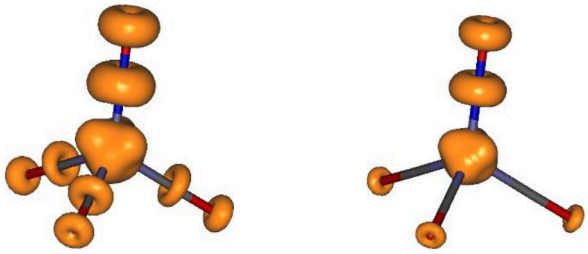

Figure 7. The $\rho_{FOD} = 0.005$ e a_0^{-3} (left) and 0.008 e a_0^{-3} (right) surface of $[Fe(CO)_3(NO)]^-$. Occupation of the two equivalent Fe–NO π-bonds and antibonds: 1.78 and 0.12; for a TPSSh-based FOD analysis see Ref. [35b].

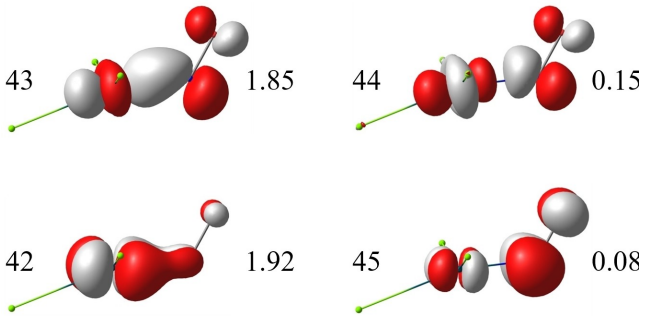

Figure 8. Bond/antibond couples in $[PdCl_3(NO)]^{2-}$. HOMO−1 (MO 42), HOMO (MO43), LUMO (MO 44) and LUMO + 1 (MO45) from a CASSCF(4,4) approach. Surfaces are drawn at an isovalue of 0.08 atomic units; the occupation of each MO is given.

for bent-bonded metal nitrosyls, the HOMO, the M–NO σ-bond, is depopulated to some extent with the corresponding antibond populated accordingly. The HOMO−1, the M–NO π-bond, shares this behaviour to a lesser extent. This result, which is common to metal nitrosyls, mirrors a peculiarity of the ligand which, as an acceptor ligand, uses its N–O-π* orbitals for the M–NO bonds. The N–O-π*-antibonds share their space with the occupied N–O-π bonds. As a consequence, the M–NO bonds experience Pauli repulsion with those N–O-π bonds which results in a weakened, partly dissociated M–NO interaction. Computationally, partial dissociation is equivalent to static correlation, the extent of which may be directly guessed by the occupation of the M–NO antibond. All these aspects are known and well documented for metal–nitrosyl bonding. For a bent $\{CoNO\}^8$ which shares a singlet ground state with the palladium species of this work, an appendix in Ref. [23d] gives a tutorial-style example.

However, there are some aspects which distinguish $\{M(NO)_n\}^{10}$ species from nitrosyls with less than ten electrons. Hence, a characteristic is encountered on attempts to enlargen the active space. In case of $[PdCl_3(NO)]^{2-}$, the remaining three 4d-orbitals of the central metal may be added which results in a (10,7) space that includes all "Enemark-Feltham electrons". As a result, the three additional MOs refine to occupation numbers of more than 1.998 (with the occupations of the four MNO-related MOs being unaltered). Obviously, $\{M(NO)_n\}^{10}$ species show, to some extent, the typical subshell contraction of d^{10} species.

Similar numbers were obtained for the binuclear $[Pd_2Cl_4(NO)_2]^{2-}$ anion (bond/antibond occupation: σ 1.85/0.15, π 1.93/0.07) in a CASSCF(8,8) approach.

For $[NiCl_2(NO)_2]$, a result was obtained which underlines the significance of subshell contraction even more pronouncedly. Here, the minimal reasonable active space contains the eight electrons of four Ni–NO bonding and four antibonding interactions. The occupation numbers in this (8,8) space maybe divided into σ- and π-Ni–NO interactions. In fact, only the σ–type bonds and antibonds (occupations: 1.60, 1.57, 0.43, 0.41) show the typical situation of partially dissociated bonds at considerable overlap. The potential Ni–NO π-bonds, however, remain Ni lone pairs, practically no overlap is established (occupations: 1.98, 1.98, 0.02, 0.01).

For the reference {MNO}^{10} nitrosyl, $[Fe(CO)_3(NO)]^-$, the result is slightly different since its co-ligands are, though weaker, acceptor ligands as well. But also here, the expansion of the active space changes the description of the M–NO bond only marginally [see Ref. [35c] for (4,4) and (10,10) approaches, and Ref. [39] for a (14,14) active space].

{NiNO}^{10} species complement these findings. As requested by a reviewer, we may include species from Ref. [40] (an electroneutral tetracoordinate complex with a linear Ni–N–O function and a hydridotrispyrazolylborate coligand) and Ref. [41] (related complexes with linear nitrosylnickel moieties as well as bent NiNO species with chlorido and phosphane coligands). In the former work, CASSCF calculations show the same result as above: a (4,4) active space refines to occupation numbers different from zero and two, whereas enlarged spaces do not contribute more truly active MOs. The computational description in the latter work is limited to a DFT treatment. The result illustrates an analysis by Radon who investigated the trace of static correlation in DFT approaches: as shown above for the dinitrosylnickel complex, hybrid functionals may refine to broken-symmetry solutions to capture the partial dissociation of the Ni–NO bonds in terms of an open-shell biradical state.

Eventually, the peculiarities of closed subshells become obvious in an impressive way for the above-mentioned $[CuCl_3(NO)]^-$ ion. Though a CASSCF(12,12) approach was chosen, a (2,2) active space containing a Cu–NO bond and its antibond represent the MR character, leaving all other MOs with occupations of practically two or zero.[24]

(6) Static correlation and DFT results

The broken-symmetry issue of the last nickel example already pointed to the effect of static correlation in a DFT framework using hybrid functionals. For the GGA functional BP86 which has been used above for structure optimisation, the closed-shell singlet wave function proved to be stable. However, there is a trace of the partial dissociation. As pointed out above, M–NO bond lengths are typically computed too short in such a case. (Notably, we used BP86 because of its capability to reproduce IR spectra as well as structural parameters except the special case of M–NO distances.) How does the use of a CASSCF wavefunction alter the M–NO bond description? Table 10 collects some informative values for the mononuclear $[PdCl_3(NO)]^{2-}$ ion by comparing BP86 and all-electron-CASSCF numbers. In terms of EOS-R values, both approaches show the largely covalent character of the Pd–NO bond (100% meaning clearly heteropolar bonds with 50% as the limit of perfect covalence). Here, the multireference wave function resulted in the OS assignment $Pd^0(NO)^+$ as well, but did so in a really borderline way.

Table 10. $[PdCl_3(NO)]^{2-}$. Charges and effective oxidation states using a TFVC (topological fuzzy Voronoi cells) partitioning by the Apost-3D program (note the differences to the QTAIM partitioning of Table 1).

	BP86	CASSCF(4,4)
Q_{TFVC}(Pd)/*e*	0.62	0.94
Q_{TFVC}(NO)/*e*	−0.43	−0.48
Q_{TFVC}(*trans*–Cl)/*e*	−0.82	−0.89
Q_{TFVC}(*cis*–Cl)/*e*	−0.68	−0.78
EOS_{Pd}, EOS_{NO} (*R*/%)	0, +1 (62.4)	0, +1 (51.0)

Appendix II

Do matching Pd-XAS features of PdCl(NO) and $PdCl_2$ prove the same oxidation state of Pd?

The authors of Ref. [14] state in their work on PdCl(NO): "According to the XAS spectrum the charge located at palladium is comparable to that of $PdCl_2$ or PdO." A referee went a step further and stated: "… one would assign an OS of II to the Pd, as nicely demonstrated by XAS …". This latter statement is contradictory to the analysis presented in this work and raises the question of whether the deduction of an OS from a charge-sensitive experiment is justified or not. In the introduction of a recent work on OSs by the Salvador and Head-Gordon groups we find a guide. The authors state: "… the OS of an atom is not itself a precisely defined observable. It *may* correlate with observables such as X-ray absorption spectral shifts, but this requires calibration."[42] In order to clarify whether the required calibration was observed in the case above, we develop the relationship between charge and OS starting from the latter.

In 2016, the IUPAC defined the concept "oxidation state": *The oxidation state of an atom is the charge of this atom after ionic approximation of its heteronuclear bonds.*[19c] Being defined that way, the OS equals, for ionic compounds, the respective atom's charge which may be probed by methods such as XAS. At the same time, for non-ionic compounds, the OS is a mental construct which deviates from the actual partial charge. Thus, the above-mentioned calibration is needed as a bridge between experiment and the OS concept. To clarify our Pd issue, two scenarios explain a difference between an atom's OS and its charge: the multiple-bond scenario and the acceptor-ligand scenario.

The first scenario considers the consequences of more than one bond to an element of interest. In a simple case such as HCl there is one bond to assign in the course of the ionic approximation. As a result, the OS is a nearest integer of the charges of the two elements. For NH_3, we have three bonds to assign. In the ionic approximation, all the electrons go to the more electronegative N and an OS of −III results. However, the nearest-integer rule is no longer valid. Both DFT and WFT methods (we checked BP86/def2-TZVP and CASSCF(8,7)/def2-QZVPP, the latter including all valence electrons), give a QTAIM nitrogen charge *Q*/*e* of about −1 (DFT −1.025, WFT −1.068), two electrons less than the OS. Notably, a charge-sensitive experimental method would 'see' this −1 charge, not the −III OS.

The second scenario deals with the bonding of a central metal to an acceptor ligand via backbonds. Backbonds efficiently pull electron density away from a central metal. However, for the usually metal-centred backbonds, their electrons go to the metal on OS assignment despite the marked transfer of electron density to the acceptor ligand. Both scenarios culminate in carbonyl and nitrosyl complexes: CO as well as NO^+ are electron-withdrawing ligands each of which accepts two backbonds from a central metal.

$[Fe(CO)_3(NO)]^-$: can a charge Q_{Fe}/e of almost +1 be compatible with an OS_{Fe} of −II?

We can check these facts for a couple of well-known species for which all the required numbers are available including an X-ray-spectroscopic investigation. Thus, Ref. [23d] provides us with DFT-derived QTAIM charges Q_{Fe}/e of the iron central atom in the species $[Fe(CO)_4]^{2-}$ (+0.64) and $[Fe(CO)_3(NO)]^-$ (+0.81).[23d] The value for the $[Fe(CO)_4]^{2-}$ anion shows all the issues described above. Thus, the charge of +0.64 approximates not even roughly the OS_{Fe} of −II due to a marked imbalance of electron-density losses and gains. Indeed, the loss from the $3d^{10}$ subshell through eight Fe-to-CO π-backbonds exceeds the inflow into empty 4s/4p orbitals through four CO-to-Fe σ-donor bonds by far. Since NO^+ is both a stronger acceptor and a weaker donor than CO, the QTAIM charge of the iron central atom is even a bit higher for the isoelectronic $[Fe(CO)_3(NO)]^-$. X-ray-spectroscopic features mirror the close resemblance of charges and orbital occupations of the isoelectronic species $[Fe(CO)_4]^{2-}$ and $[Fe(CO)_3(NO)]^-$.[35b] The scenario 1 and 2 parameters are largely equal for these isoelectronic species which makes the dianion an adequate reference for the nitrosyl complex. Hence, the demand of proper calibration (see above) seems to be met here and the same OS of −II may be deduced for the nitrosyl species as well. However, we should recall IUPAC's OS definition to see that an existing charge/OS correlation does not make this OS an experimentally determined quantity. The ionic approximation of the heteronuclear bonds of a non-ionic species needs the (experimentally inaccessible) assignment of each bond to the bonding partner with the higher share. In fact, the computational tool applied here, EOS analysis, confirms the OS −II for the Fe central atom of both species, together with a marked covalence of the Fe–NO interaction as a caveat that a borderline situation is reached.

The Pd case

Unlike the ferrate example where reference and 'sample' are closely related isoelectronic species, severe problems arise on attemps to deduce an OS from charges if the electronic situation of central atoms in different environments is compared, impeding a reliable calibration. $PdCl_2$ and PdCl(NO) provide a typical couple. The OS of Pd in $PdCl_2$ is +II whereas the charge of Pd is expected to be $+2-x$, with an x that takes the actual degree of Pd–Cl covalency into account. The prediction of the charge of Pd in PdCl(NO) is less straightforward due to the occurrence of both polar Pd–Cl bonds and Pd-to-NO backbonds. A quantitative treatment clarifies this issue. For solid PdCl(NO), Evers *et al.* report +0.59 for the QTAIM charge Q_{Pd}/e, close to the values of molecular {PdNO}[10] species in Tables 1 and 2. For a comparison with $PdCl_2$, we chose the molecular polymorph β-$PdCl_2$.[43] The X-ray parameters of the Pd_6Cl_{12} cluster in β-$PdCl_2$ are reliably reproduced on the BP86/def2-TZVP + D3 level of theory (d_{Pd-Cl}/Å: X-ray 2.310, DFT 2.325). The QTAIM charge of the Pd atom is computed as +0.61, truly close to the values of the NO-containing species.[44] As a result, a charge-sensitive experimental method such as XAS may show coincidence of the decisive spectral features. However, due to the presence of backbonds in the nitrosyl species, no serious conclusion on OSs can be drawn. It is the EOS method which clarifies the scene. Despite the +0.61 charge of palladium(II) chloride which mirrors a partial covalence of the Pd–Cl bonds, the OS is clearly +II (R = 78 %). Hence, the situation is different from that of the chlorido-nitrosyl-palladium species, for which a (borderline, R approaching 50 %) Pd^0/NO^+ assignment of the OS was obtained. However, the detected covalency of the σ–Pd–NO bond made this a borderline, but sensible, result. Starting from ten electrons of a palladium(0), the strong acceptor NO^+ pulls more than one electron into its two π* orbitals and we end up, together with polar Pd^0–Cl bonds, at a charge close to that of $PdCl_2$. Notably, the markedly larger mean Pd–Cl distance of 2.557 Å in PdCl(NO) compared to 2.310 Å in $PdCl_2$ shows that the chlorido ligands experience the repulsion from the higher occupation of the $4d(x^2-y^2)$ orbital which is empty in the low-spin-d^8 compound $PdCl_2$. (The reader may consider the high occupation of all metal d-orbitals of formal d^8 complexes under inverted-ligand-field conditions.[45] Another helpful view is provided by the 'quasi-d^{10}' formalism.[46])

In conclusion, the result in Ref. [14] that the charge of the Pd in PdCl(NO) as well as some XAS features resemble that of a reference substance such as $PdCl_2$ does not justify an OS of +II for the Pd atoms of both compounds (as concluded by a reviewer). Couples of backbonds, in particular those toward the strong acceptor NO^+, go along with a marked electron-density drain away from a central metal. At the same time, backbonds do not alter a metal's OS. A large difference between the charge and charge-related experimental parameters on the one hand, and an OS in its IUPAC definition on the other, is thus not an issue but is immanent in the concept. To get to the heart of the controversy: for non-ionic species, there is no 'experimental oxidation state'.

Acknowledgements

We are indebted to Dr. Ralf Köppe, KIT Karlsruhe, for a QTAIM analysis of α-$PdCl_2$. Open Access funding enabled and organized by Projekt DEAL.

Conflict of Interest

The authors declare no conflict of interest.

Data Availability Statement

The data that support the findings of this study are available in the supplementary material of this article.

[1] W. Beck, G. Fischer, M. Göbel, J. Evers, T. M. Klapötke, *Z. Anorg. Allg. Chem.* **2013**, *639*, 1332–1339.
[2] J. H. Enemark, R. D. Feltham, *Coord. Chem. Rev.* **1974**, *13*, 339–406.
[3] W. Beck, K. Lottes, *Chem. Ber.* **1965**, *98*, 2657–2673.
[4] a) J. Smidt, R. Jira, *Chem. Ber.* **1960**, *93*, 162–165; b) J. H. MacNeil, P. K. Gantzel, W. C. Trogler, *Inorg. Chim. Acta* **1995**, *240*, 299–304.
[5] C. C. Addison, B. F. G. Johnson, *Proc. Chem. Soc.* **1962**, 305–306.
[6] a) W. Manchot, A. Waldmüller, *Ber. Dtsch. Chem. Ges.* **1926**, *59*, 2363–2366; b) J. R. Partington, A. L. Whynes, *J. Chem. Soc.* **1949**, 3135–3141; c) W. P. Griffith, J. Lewis, G. Wilkinson, *J. Chem. Soc.* **1959**, 1775–1779.
[7] Z. Iqbal, T. C. Waddington, *J. Chem. Soc. A* **1969**, 1092–1093.
[8] W. Hieber, A. Jahn, *Z. Anorg. Allg. Chem.* **1959**, *301*, 301–310.
[9] J. Conradie, A. Ghosh, *Inorg. Chem.* **2014**, *53*, 4847–4855.
[10] a) W. Beck, T. M. Klapötke, P. Mayer, *Z. Anorg. Allg. Chem.* **2006**, *632*, 417–420; b) W. Beck, A. Enzmann, P. Mayer, *Z. Anorg. Allg. Chem.* **2005**, *631*, 105–109; c) L. F. Dahl, E. Rodulfo de Gil, R. D. Feltham, *J. Am. Chem. Soc.* **1969**, *91*, 1653–1664.
[11] J. Bohnenberger, I. Krossing, *Angew. Chem. Int. Ed.* **2020**, *59*, 5581–5585; *Angew. Chem.* **2020**, *132*, 5629–5633.
[12] a) X. Wang, M. Zhou, L. Andrews, *J. Phys. Chem. A* **2000**, *104*, 7964–7973; b) K. Hedberg, L. Hedberg, K. Hagen, R. R. Ryan, L. H. Jones, *Inorg. Chem.* **1985**, *24*, 2771–2774; c) L. Hedberg, K. Hedberg, S. K. Satija, B. I. Swanson, *Inorg. Chem.* **1985**, *24*, 2766–2771.
[13] M. Schmitt, M. Mayländer, J. Goost, S. Richert, I. Krossing, *Angew. Chem. Int. Ed.* **2021**, *60*, 14800–14805; *Angew. Chem.* **2021**, *133*, 14926–14931.
[14] J. Evers, T. M. Klapötke, W. Beck, M. B. R. Völkl, G. Oehlinger, R. Köppe, A. Zimina, S. Wolf, *Z. Anorg. Allg. Chem.* **2022**, e202200337.
[15] J. Cámpora, P. Palma, D. del Río, E. Carmona, C. Graiff, A. Tiripicchio, *Organometallics* **2003**, *22*, 3345–3347.
[16] a) T. A. Stromnova, D. V. Paschenko, L. I. Boganova, M. V. Daineko, S. B. Katser, A. V. Churakov, L. G. Kuz'mina, J. A. K. Howard, *Inorg. Chim. Acta* **2003**, *350*, 283–288; b) T. A. Stromnova, M. V. Dayneko, A. V. Churakov, L. G. Kuz'mina, J. Cámpora, P. Palma, E. Carmona, *Inorg. Chim. Acta* **2006**, *359*, 1613–1618.
[17] R. E. Podobedov, T. A. Stromnova, A. V. Churakov, L. G. Kuzmina, I. A. Efimenko, *J. Organomet. Chem.* **2010**, *695*, 2083–2088.
[18] a) L. Zhao, M. Zhi, G. Frenking, *Int. J. Quantum Chem.* **2021**, e26773; b) E. Kraka, W. Zou, Y. Tao, *WIREs Comput. Mol. Sci.* **2020**, *10*, e1480.
[19] a) P. Karen, P. McArdle, J. Takats, *Pure Appl. Chem.* **2014**, *86*, 1017–1081; b) P. Karen, *Angew. Chem. Int. Ed.* **2015**, *54*, 4716–4726; *Angew. Chem.* **2015**, *127*, 4798–4809; c) P. Karen, P. McArdle, J. Takats, *Pure Appl. Chem.* **2016**, *88*, 831–839.
[20] A. Haaland, *Angew. Chem. Int. Ed. Engl.* **1989**, *28*, 992–1007.
[21] a) E. Ramos-Cordoba, V. Postils, P. Salvador, *J. Chem. Theory Comput.* **2015**, *11*, 1501–1508; b) V. Postils, C. Delgado-Alonso, J. M. Luis, P. Salvador, *Angew. Chem. Int. Ed.* **2018**, *57*, 10525–10529; *Angew. Chem.* **2018**, *130*, 10685–10689; c) M. Gimferrer, J. Van der Mynsbrugge, A. T. Bell, P. Salvador, M. Head-Gordon, *Inorg. Chem.* **2020**, *59*, 15410–15420.
[22] E. Ramos-Cordoba, P. Salvador, I. Mayer, *J. Chem. Phys.* **2013**, *138*, 214107.
[23] a) A. Hasil, D. Beck, D. Schröder, S. Pillet, E. Wenger, T. Woike, P. Klüfers, D. Schaniel, *Angew. Chem. Int. Ed.* **2022**, *61*, e202210671; b) J. Popp, T. Riggenmann, D. Schröder, T. Ampßler, P. Salvador, P. Klüfers, *Inorg. Chem.* **2021**, *60*, 15980–15996; c) T. Ampßler, G. Monsch, J. Popp, T. Riggenmann, P. Salvador, D. Schröder, P. Klüfers, *Angew. Chem. Int. Ed.* **2020**, *59*, 12381–12386; *Angew. Chem.* **2020**, *132*, 12480–12485; d) J. Popp, P. Klüfers, *Eur. J. Inorg. Chem.* **2022**, *2022*, e202200374.
[24] J. K. Bower, A. Y. Sokolov, S. Zhang, *Angew. Chem. Int. Ed.* **2019**, *58*, 10225–10229; *Angew. Chem.* **2019**, *131*, 10331–10335.
[25] a) F. Neese, *Wiley Interdisciplinary Reviews: Computational Molecular Science* **2018**, *8*, e1327; b) F. Neese, *Wiley Interdisciplinary Reviews: Computational Molecular Science* **2012**, *2*, 73–78.
[26] F. Weigend, R. Ahlrichs, *Phys. Chem. Chem. Phys.* **2005**, *7*, 3297–3305.
[27] F. Weigend, *Phys. Chem. Chem. Phys.* **2006**, *8*, 1057–1065.
[28] a) A. D. Becke, *Phys. Rev. A* **1988**, *38*, 3098–3100; b) J. P. Perdew, *Phys. Rev. B* **1986**, *33*, 8822–8824.
[29] a) S. Grimme, J. Antony, S. Ehrlich, H. Krieg, *J. Chem. Phys.* **2010**, *132*, 154104; b) S. Grimme, S. Ehrlich, L. Goerigk, *J. Comput. Chem.* **2011**, *32*, 1456–1465.
[30] V. Barone, M. Cossi, *J. Phys. Chem. A* **1998**, *102*, 1995–2001.
[31] F. Neese, F. Wennmohs, A. Hansen, U. Becker, *Chem. Phys.* **2009**, *356*, 98–109.
[32] W. Zou, Y. Tao, M. Freindorf, M. Makos, N. Verma, E. Kraka, *Dallas* **2020**.
[33] T. Lu, F. Chen, *J. Comput. Chem.* **2012**, *33*, 580–592.
[34] P. Salvador, E. Ramos-Cordoba, M. Gimferrer, M. Montilla, *Universitat de Girona, Spain* **2010**.
[35] a) M. Gruden, M. Zlatar, *Theor. Chem. Acc.* **2020**, *139*, 126; b) L. Burkhardt, Y. Vukadinovic, M. Nowakowski, A. Kalinko, J. Rudolph, P.-A. Carlsson, C. R. Jacob, M. Bauer, *Inorg. Chem.* **2020**, *59*, 3551–3561; c) J. E. M. N. Klein, B. Miehlich, M. S. Holzwarth, M. Bauer, M. Milek, M. M. Khusniyarov, G. Knizia, H.-J. Werner, B. Plietker, *Angew. Chem. Int. Ed.* **2014**, *53*, 1790–1794; *Angew. Chem.* **2014**, *126*, 1820–1824.
[36] J. Shee, M. Loipersberger, D. Hait, J. Lee, M. Head-Gordon, *J. Chem. Phys.* **2021**, *154*, 194109.
[37] a) M. Feldt, Q. M. Phung, *Eur. J. Inorg. Chem.* **2022**, *2022*, e202200014; b) Q. M. Phung, M. Feldt, J. N. Harvey, K. Pierloot, *J. Chem. Theory Comput.* **2018**, *14*, 2446–2455; c) W. Jiang, N. J. DeYonker, A. K. Wilson, *J. Chem. Theory Comput.* **2012**, *8*, 460–468.
[38] a) S. Grimme, A. Hansen, *Angew. Chem. Int. Ed.* **2015**, *54*, 12308–12313; *Angew. Chem.* **2015**, *127*, 12483–12488; b) A. Bauer Christoph, A. Hansen, S. Grimme, *Chem. Eur. J.* **2017**, *23*, 6150–6164.
[39] G. Monsch, P. Klüfers, *Angew. Chem. Int. Ed.* **2019**, *58*, 8566–8571; *Angew. Chem.* **2019**, *131*, 8654–8659.
[40] N. C. Tomson, M. R. Crimmin, T. Petrenko, L. E. Rosebrugh, S. Sproules, W. C. Boyd, R. G. Bergman, S. DeBeer, F. D. Toste, K. Wieghardt, *J. Am. Chem. Soc.* **2011**, *133*, 18785–18801.
[41] S. Soma, C. Van Stappen, M. Kiss, R. K. Szilagyi, N. Lehnert, K. Fujisawa, *J. Biol. Inorg. Chem.* **2016**, *21*, 757–775.
[42] M. Gimferrer, A. Aldossary, P. Salvador, M. Head-Gordon, *J. Chem. Theory Comput.* **2022**, *18*, 309–322.
[43] D. B. Dell'Amico, F. Calderazzo, F. Marchetti, S. Ramello, *Angew. Chem. Int. Ed. Engl.* **1996**, *35*, 1331–1333.

[44] In Ref. 14, the α-polymorph of $PdCl_2$ was used as the reference for the XAS investigation. We are indebted to Dr. Ralf Köppe, KIT Karlsruhe, for the calculation of the QTAIM charges of this α-$PdCl_2$ reference. The applied methodology was described in Ref. 14. The result was $Q_{Pd}/e = 0.61$ if both the lattice and the atomic positions were refined, and $Q_{Pd}/e = 0.63$ if the lattice was kept constant at the experimental values.
[45] R. Hoffmann, S. Alvarez, C. Mealli, A. Falceto, T. J. Cahill, T. Zeng, G. Manca, *Chem. Rev.* **2016**, *116*, 8173–8192.
[46] I. F. Leach, R. W. A. Havenith, J. E. M. N. Klein, *Eur. J. Inorg. Chem.* **2022**, e202200247.

Manuscript received: October 17, 2022
Revised manuscript received: January 11, 2023
Accepted manuscript online: January 14, 2023

